COMPUTATIONAL FLUID DYNAMICS MODELING APPROACH TO EVALUATE VSC–17 DRY STORAGE CASK THERMAL DESIGNS

Kaushik Das,[*] Debashis Basu,[*] Jorge Solis,[**] Ghani Zigh[**]

Center for Nuclear Waste Regulatory Analyses
Southwest Research Institute®
San Antonio, Texas 78238

****U.S. Nuclear Regulatory Commission***
Washington, DC 20555-0001

Abstract

A numerical simulation of flow and heat transfer in a ventilated concrete dry storage cask system–17 (VSC–17) is performed and results compared with experimental data to assess the validity of the computational approach. The measurements of steady state temperature distributions on the cask surface, concrete surface, air flow channels, and fuel canister guide are available. Numerical simulations were carried out for normal operating conditions, where both the inlet and outlet vents are open, and for off-normal condition when normal air circulation is interrupted because of blocked vents. Results include the flow and temperature pattern in the ventilated storage system. Computed results were compared with experimental data for axial temperature distribution along the fuel assembly and radial temperature distribution along the storage assembly system. The effect of the turbulence model on temperature distribution pattern was also studied. For all the simulated cases, the computed results showed a trend similar to the experimental observation but did not model exactly. Computed peak cladding temperature in all the simulation cases was slightly higher than the experimental data. Heat transfer results showed some variation due to difference in backfill gas. A study of different k-ε and k-ωturbulence models showed very little effect on temperature distribution.

1. INTRODUCTION

A ventilated storage cask operates on the basic principles of buoyancy driven natural convection, where cooler air enters the air passage near the bottom of the system, absorbs decay heat, and the lower density hot air exits the system near the top. Under normal operating conditions, the majority of decay heat is dissipated through natural convection of coolant air flow through the passage. However, radiation, dissipated heat convection, and conductive heat transfer at the outer cask surface also helps eject heat. At off-normal operating conditions, where the inlet or outlet of the air passage is blocked, heat transfer at the outer surface becomes the principal method of energy dissipation. To ensure safe and reliable operation of a spent fuel storage system at normal and off-normal conditions by maintaining the peak cladding temperature (PCT) at or below the allowable limit, a proper understanding of the associated flow and heat transfer mechanisms are required. In recent years, engineers are relying increasingly on computational fluid dynamics (CFD) tools to address critical heat transfer issues of spent fuel casks and canisters and estimate safety margins. Simulation results obtained from such studies indicate that temperature distribution depends on a number of factors including proper choice of modeling techniques, assumptions, and physical parameters such as turbulence models, material properties, and heat transfer coefficients. Hence, proper choice of modeling parameters and techniques are important for performing reliable simulations and for assessing the uncertainty of simulation results.

Researchers have pointed out that heat transfer in a storage cask is a complicated process due to the inherent geometrical complexity and the combined convection-radiation process induced by thermal radioactive process (Heng et al., 2002). Other factors contributing to the

overall heat transfer include the spent-fuel heat generation rate, thermal boundary condition, canister backfill media, and cask orientation with respect to gravity that dictates natural convection pattern. Prior studies (Nishimura et al., 1996; Shibazaki et al., 1998) showed that the convective heat transfer in a storage cask depends strongly on the Grashof and Prandtl numbers and some geometrical parameters. Early investigations (Arya and Keyhani, 1990; Cannan and Klein, 1998) focused on natural convection within the spent-fuel assemblies. Recent investigation by Heng et al. (2002) found that with an increase in the Rayleigh number, the dominant heat transfer mode changes from conduction to convection. Heng et al. (2002) also determined that in the limit of the turbulent Rayleigh number, convective heat transfer is so strong that the temperature change mainly occurs near the wall of the cask, and the natural convection on local scale plays a more important role than that of global scale. Greiner et al. (2007) performed two-dimensional analyses of transportation casks and investigated two different thermal conductivity models to represent the basket that holds the fuel assembly. Araya and Greiner (2007) performed two-dimensional simulations of a boiling water reactor (BWR) fuel assembly within an isothermal enclosure for Nitrogen and Helium backfill. They found that natural convection is significant at lower basket temperatures with Nitrogen backfill, whereas, for Helium backfill, natural convection has no significant effect in reducing temperature. Li et al. (2007) studied three different models to calculate PCT of a storage or transportation cask with different backfill gas and vacuum condition in the canister. The study concluded that under vacuum condition, PCT limit is exceeded at a lower boundary temperature. Chalasani et al. (2007) conducted experimental and numerical analyses of horizontal and vertical arrays of heated rods inside an isothermal enclosure to mimic conditions encountered in a BWR fuel assembly between two consecutive spacer plates. Gudipati and Greiner (2007) conducted two-dimensional numerical studies of multipurpose canisters and compared different approaches to model the internal components. Waturu et al. (2008) performed heat transfer analysis of reinforced concrete storage casks and concrete filled steel casks using the FIT-3D® thermal hydraulics code and the commercial solver PHOENICS®. Their computed temperature values at the canister and convective air flow velocities were compared with experimental data (Takeda et al. 2008). Results showed that a hybrid thermal hydrolics and CFD approach can provide reasonable temperature estimates. Lee et al. (2009) performed a detailed experimental and computational analysis of a vertical storage system that was comprised of a stainless steel canister with concrete overpack under normal and off-normal conditions. The computational model employed an effective thermal conductivity approach proposed by Wooton and Epstein (1963) in conjunction with a porous media approximation to model the fuel rods. The simulation results showed temperature distribution contours at different cross sectional location and coolant air velocity contours. Some researchers have carried out numerical studies of the VSC–17 cask system. Walavalkar and Schowalter (2004) performed a CFD analysis of the VSC–17 spent fuel dry storage system using the FLUENT® software. The flow equations with turbulence and energy equations with thermal radiation were solved for a 90-degree section of the VSC–17 system. They concluded that CFD provides an excellent tool for waste management given the proximity of predicted results with experimental data.

From the review of open literature, it is clear that computed PCT values depend on the choice of certain physical and modeling parameters in the system such as operating density, turbulence, and inlet temperature. In the present study, a comprehensive thermal analysis is performed to investigate the effect of these parameters on predicted temperature distribution of a vertical storage system. More specifically, the effect of backfill gas, turbulence models, and input parameters for natural convection such as operating density is analyzed. Simulations were also carried out for off-normal conditions where the inlet or outlet vents were artificially blocked to limit or eliminate coolant air supply. Computed results show axial temperature distribution along the fuel assemblies and radial temperature distribution at different vertical heights across the domain. Results are also presented for temperature contours at different cross sectional planes. Computed results under different scenarios are compared with experimental data of McKinnon et al. (1992). A principal objective of the

study is to validate the numerical simulation approach against available experimental data for different backfill gases and vent block conditions. In addition, a number of Reynolds Averaged Navier Stokes Equations (RANS)-based turbulence models were assessed and compared based on their effectiveness in predicting the temperature field.

2. DESCRIPTION OF THE STORAGE SYSTEM

The VSC–17 system has the capacity to store 17 canisters of consolidated nuclear fuel. It has two major components: a multi-assembly sealed basket (MSB) and a ventilated concrete cask (VCC). The MSB has a steel cylinder containing the guide sleeve assembly that holds the canisters with fuel rods. The MSB cavity is backfilled with either Nitrogen or Helium gas to create an inert atmosphere that enhances heat transfer from fuel assemblies and at the same time prevents fuel oxidation and basket component corrosion. A composite shield lid provides sealing to the MSB contents. The VCC is a concrete shell with an inner steel liner and a weather cover. VCC encloses the MSB with an annular gap between the outer surface of the MSB and inner surface of the VCC. This gap provides conduit for the coolant air that enters the system through an inlet at the bottom and leaves through an exhaust at the top. The coolant airflow is driven by natural convection and dissipates the decay heat into the open atmosphere. The geometry of the VSC–17 system and component description, along with experimental details, are provided in the report of McKinnon et al. (1992).

3. DOMAIN AND GRID

The computational domain consisted of a quadrant of the whole circular cross section of the storage cask. Symmetry is assumed at the edge of the quadrants. The heat load distribution shows that the assumption is reasonable as the rate of decay heat generation is almost the same in each quadrant. Though simulation of the full cross sectional area will likely yield more accurate results, symmetry is assumed in the present study to achieve computational economy—schematic of the domain is shown in Figure 1(a) and (b). The computational domain consisted of the cask geometry but did not include the surrounding ambient environment. The computational grid consisted of 1,038,794 cells and 1,166,560 nodes. Special consideration was given to the mesh spacing between the VCC liner and MSB outer shell for air flow through this annular gap. In the near-wall region, the mesh was chosen to use the enhanced wall function formula to bridge the viscosity-affected region between the walls and the fully turbulent core region. The y^+ for the first grid point was of the order of 0.75. Geometry of the VSC–17 cask with the computational grid is shown in Figure 2(a) and (b). Figure 3 highlights the computational grid at the mid-vertical plane of the domain. It also shows that a combination of hexahedral and tetrahedral mesh was used to represent the complex geometrical pattern.

4. NUMERICAL MODELING

The commercial CFD package FLUENT® version 6.3 is used in the present analysis. Solution was obtained for the steady-state incompressible Navier-Stokes equations. The pressure based solver of FLUENT was used in conjunction with a Green-Gauss, cell-based gradient option. An implicit time-marching scheme was used for faster convergence. The SIMPLE algorithm was used to obtain pressure velocity coupling. Details of the governing equations and numerics can be found in FLUENT® theory guide and users manual (Fluent, Inc., 2007a, b).

4.1 Radiation

For thermal radiation modeling within the VSC–17 system, the discrete ordinate model was chosen. In this approach, the radiative transfer equation for an absorbing, emitting, and scattering medium is solved for a finite number of discrete solid angles. For the present study,

four angular discretizations were used in each direction of the spherical coordinates system for the radiative transfer equations.

4.2 Turbulence

Based on the flow velocity and the dimensions, air flow in the inlet and outlet vents and annular gap between the MSB and the concrete outer shell is expected to be in the transitional regime. The calculated Reynolds number was close to the critical Reynolds number of 2,300. Hence, an appropriate turbulence model was needed for accurate prediction of natural convection flow and heat transfer. A number of turbulence models were studied to understand the choice in predicting PCT. The models tested include the standard k-ω model, the renormalization group k-ε model, the shear stress transport k-ω model, and the realizable k-ε model.

4.3 Boundary Conditions

Ambient air was excluded from the computational domain. The external boundary conditionof the cask surface was specified as convection-to-ambient air on all the cask walls except at the bottom. Radiation from the external side and top walls were also considered. On the bottom wall, conduction through the base to a concrete pad and its underlying soil was specified by defining appropriate thermal resistance. Solar insolation was neglected because the experiment was conducted indoors. The convective and radiative heat transfer boundary condition in the model was implemented by proper specification of heat transfer coefficient, emissivity, and far field ambient temperature. The heat transfer coefficients are based on standard correlations of convective heat transfer (Churchill and Chu, 1975). The surface emissivity was obtained from the standard material property (McAdams, 1954). Inside the cask, coupled boundary conditions were used at the solid–fluid interface. Thermal radiation properties and resolution control for the view factor calculations were set via internal boundary conditions on solid cells adjacent to fluid (gas) cells.

4.4 Effective Thermal Conductivity

It is assumed that there will be negligible convective flow inside the tightly packed fuel rods within the stainless steel fuel canister, which are modeled as a homogeneous solid material region with a specified uniform heat generation rate and an effective thermal conductivity; however, the canister was assumed to have anisotropic thermal conductivity. Different effective conductivities of the fuel region in the axial and radial directions were specified in FLUENT (Fluent, Inc., 2007b). For axial heat transfer, effective axial conductivity was represented as an area-weighted fraction of the cladding material conductivity and by ignoring the presence of fill gas. This relationship was implemented in FLUENT as a temperature-dependent thermal conductivity function of cladding material using an orthotropic distribution. In the radial direction, the effective thermal conductivity method (Bahney and Lotz, 1996) was used to obtain the conductivity of the fuel as a function of temperature.

4.5 Modeling Heat Generation Inside the Fuel Cans Using Source Terms

The decay heat for a given fuel can was obtained from the experimental configuration. It was applied as a uniform volumetric heat generation rate throughout the homogeneous region, modified only to include an axial power profile based on the measured axial power distribution in each individual fuel can. The axial variation of heat load was implemented as a user-defined function in the solver.

4.6 Material Properties

Thermal properties for the solid materials in the VSC–17 were obtained from experimental tests (McKinnon et al., 1992). Gas properties for air, helium, and nitrogen were determined using functions provided in the FLUENT (Fluent, Inc., 2007b) material set and Chase (1985).

5. RESULTS AND DISCUSSIONS

McKinnon et al. (1992) conducted experimental studies to see the effect of vent closure and backfill gas. The study reports nine test runs that yielded a large number of thermocouple temperature data. Temperatures were recorded inside the fuel cans, within the basket structure, and on the inner and outer surface of the VCC structure. Out of the nine experimental test conditions, four test cases were selected for the present study, which is described in Table 1. A selection was made to cover two different backfill gases, which are (i) Helium, and (ii) Nitrogen. Three different vent conditions were chosen, which are (i) open, (ii) inlet blocked, and (iii) both inlet and outlet blocked. Simulation input conditions and modeling parameters for internal MSB pressure, heat load, and atmospheric pressure were adopted from corresponding experimental observation. For all the runs described in Table 1, the transitional shear stress transport (SST) k-ω turbulence model was used. In addition, a companion study was performed to understand the effect of turbulence on temperature distribution. Conditions specified for Case–1 in Table 1 are used for this study, and the following four turbulence models were tested, (i) Standard k-ω model, (ii) Renormalization group k-ε model, (iii) Realizable k-ε model, and (iv) Transitional SST k-ω model.

Table 1: Test Conditions for the Validation Study

Case Number Condition	Case–1	Case–2	Case–3	Case–4
Backfill	Helium	Nitrogen	Helium	Helium
Vent Condition	All Open	All Open	Inlet Blocked	All Blocked

In the present simulations, the specified operating density corresponds to the inlet condition, except for Case–3 where the inlet and outlet boundary was blocked. For this case, the operating density was approximated as the initial air fill value. Simulated results for the temperature profiles are compared with the experimental data (McKinnon et al., 1992) for the cases described in Table 1. Axial temperature profile experimental data inside the fuel region, liner wall, and multipurpose canister wall were chosen to compare to the simulated CFD results. Additionally, radial profiles from the center of the fuel region to the periphery of the overpack concrete shield at two different elevations were used to compare the experimental data to the CFD results. Case–1 is treated as the baseline study for the simulations.

5.1 Baseline Study (Case–1)

Figure 4(a) and (b) shows the temperature contours for helium flow and the fuel rods. It is evident from the figure that the PCT occurs near the center of the canister assembly, which is consistent with previous experimental and computational studies (McKinnon et al., 1992; Walavalkar and Schowalter, 2004). Figure 5 shows the temperature contours for the outside concrete surface and the air passage between the concrete shell and steel liner. The temperatures of these components are significantly lower compared to the cladding temperature measured inside the canister. Additionally, in the simulations, the air temperature increases as it is heated and passed through the passage. The temperature of the outer concrete shell also changes with vertical distance. Figure 6 shows the fuel axial temperature distributions at three different locations and their comparisons with the experimental data for Case–1. The peak temperature is slightly overpredicted for all three locations by about 1 to 2 percent at the peak; however, the predicted temperature distribution shows qualitative agreement with the experimental data and follows the same pattern and trend. Axial temperature distributions along the fuel cans were measured at seven different locations using thermocouple lances, which are identified using the lance number in the present study. For all the lances, the temperature increases and then decreases with vertical distance; this trend

matches with experimental observation. Figure 7 shows the liner and multipurpose canister wall axial temperature distribution for Case–1. The simulations overpredicted the PCT by 5 percent even though the predicted temperature qualitatively agreed with the experimental observations. This relatively large difference is due to modeling issues related to material selection and omission of certain elements. Figure 8 shows the radial temperature distribution from the center of the MPC to the outside surface of the VSC–17 at two different elevations that show a reasonable agreement between experimental and computer data.

5.2 Nitrogen Backfill (Case–2)

Figures 9 through 11 show the results for Case–2. Figure 9 shows that the predicted fuel axial temperature distribution for the same locations described in Figure 6. The temperature distribution pattern with Nitrogen backfill is slightly different from that with Helium backfill as the maximum temperature location has shifted to a higher elevation. Predicted results are within 1–2 percent of experimental data at peak value. This feature was captured by the numerical model. It is also noticed that the calculated axial temperature matches more closely with experimental values. As seen in Figure 10, predicted temperature distributions along the liner and MSB are similar to that with Helium backfill. However, computed radial temperature distribution, highlighted in Figure 11, shows a better match with experimental data.

5.3 Effect of Inlet Blockage (Case–3)

Figures 12 through 14 show the results for Case–3, which simulates the closed inlet vent condition. Figure 12 shows that the predicted fuel axial temperature distribution is overpredicted compared to experimental data by at least 5 percent. However, unlike the two previous studies, the trend and pattern of temperature distribution matches. Temperature distributions highlighted in Figures 13 and 14 also confirm that the differences between experimental and computed data are relatively high. The apparently poor performance of the model for Case–3 is because the inlet of the vent is blocked, whereas the outlet of the vent was kept open during the experiment. The blockage condition was simulated specifying the inlet strip as a solid concrete wall and with mixed convection in the external surface of the blockage wall. The blockage condition was simulated by imposing a zero velocity at the inlet and with external mixed convection at the outlet boundary. Modeling the outlet boundary posed significant challenges. It was modeled as a pressure outlet boundary as well as a pressure inlet boundary with a significant quantity of reversed airflow for both cases. However, both these boundary conditions provided similar results. The circulating air operating density was specified corresponding to the ambient pressure and temperature.

5.4 Effect of Inlet and Outlet Blockage (Case–4)

Figures 15 through 17 show the results for Case–4, where both the inlet and outlet vents are blocked and the air inside the passage is trapped. The results for Case–3 also overpredict the temperature and deviate considerably from the experimental data. Unlike Case–3, both the inlet and outlet vents are blocked for Case–4. These conditions are simulated by specifying the vents as solid bodies and with mixed convection in the external surface of the blockage wall. Under this condition, the majority of the heat is dissipated through the external walls by mixed convection and radiation. Heat transfer also depends on the convection pattern in the annulus.

5.5 Effect of Turbulence Modeling

Figure 18 shows the effect of turbulence modeling on the fuel axial temperature distribution for operating conditions (same as Case–1 for three different locations). The four turbulence models considered were the transitional SST k-ω model, standard k-ω model, the Renormalization Group (RNG) k-ε model, and the realizable k-ε model. Figure 18 also shows that even though there is not much appreciable difference between the predictions from the three models, the RNG k-ε model and the realizable k-ε model predictions are closer to the

experimental results. Out of the three models, the RNG k-ε model-based prediction of the temperature is the closest to the experimental value. Normally, an RNG k-ε model or realizable k-ε model is best suited for flows that are dominated by recirculation, large vortices, and separation regions. Because the flow in this case is wall bounded and in the transitional region, no significant improvement is observed using the RNG k-ε model or realizable k-ε model over the standard k-ω model.

Figure 19 shows the effect of the turbulence model on the MSB temperature distribution. Similar trends can be observed in this figure, which shows that the RNG k-ε model predicts the temperature distribution closest to the experimental data. As the elevation increases, the relative difference between the peak temperatures predicted by the different models also increases. Figure 20 shows the liner temperature distribution with the different turbulence models. Among the three models, the RNG k-ε model predicts the liner temperature that is closest to the experimental data for both locations in the MSBs. The difference between the predicted result and the experimental data is the maximum for the standard k-ω model. Figure 21 shows the radial temperature distribution from the center of the MPC to the outside surface of the VSC–17 at both the elevations for the different turbulence models. All three turbulence models give approximately the same prediction. Figures 18 through 21 demonstrate that these two equations' turbulence models provide very similar results and do not affect temperature distribution in a significant way.

6. CONCLUSION

A numerical model to perform thermal analysis of the VSC–17 cask was evaluated and assessed in this study. The analysis provides a basis to validate the model construction using an off-the-shelf commercial computational fluid dynamic solver and enhance the understanding of the different modes of heat transfer (i.e., conduction, natural convection, and radiation) from fuel assemblies under normal and off-normal operating conditions. Simulated results were compared with experimental results. For all the cases, the computed results showed similar trend and pattern and matched the experimental observation in a range of 5 percent. In almost all the cases, the simulated PCT was slightly higher than the experimental data. However, the match between the computed results and the experimental data was better when Nitrogen was used as a backfill gas inside the canister as compared to Helium backfill. Simulations with a blocked vent showed higher deviation from experimental data, which can be attributed to modeling issues at blockage boundaries and outer walls. A study of different k-ε and k-ω turbulence models showed that the two different equation models provide analogous results. Though the renormalization group k-ε model produced a slightly better match, the results obtained from all the models were comparable.

7. DISCLAIMER

This paper is an independent product of the CNWRA and does not necessarily reflect the view or regulatory position of the USNRC. The NRC staff views expressed herein are preliminary and do not constitute a final judgment or determination of the matters addressed or of the acceptability of a license application for spent fuel storage or transportation systems.

8. REFERENCES

Arya, M.S., M. Keyhani, "Convective Heat Transfer in a Sealed Storage Cask Containing Spent-Fuel Canisters," *Nuclear Science and Engineering*, Vol. 105, pp. 391–403 (1990).

Araya, P.E., M. Greiner, "Two-Dimensional Simulations of Natural Convection/Radiation Heat Transfer for BWR Assembly within Isothermal Enclosure," *Proceedings of the 15th International Symposium on the Packaging and Transportation of Radioactive Materials*, Vol. 18, No. 3, pp. 171–179 (2007).

Bahney, R.H., T.L. Lotz, "Spent Nuclear Fuel Effective Thermal Conductivity Report," Prepared for the U.S.DOE, Yucca Mountain Site Characterization Project Office by TRW Environmental Safety Systems, Inc. (1996).

Canaan, R.E., D.E. Klein, "A Numerical Investigation of Natural Convection Heat Transfer Within Horizontal Spent-Fuel Assemblies," *Nuclear Technology*, Vol. 123, No. 2, pp. 193–208 (1998).

Chalsani, N.R. et al., "Simulations of Natural Convection/Radiation Heat Transfer for Horizontal and Vertical Arrays of Heated Rods Inside a Uniform Temperature Enclosure", *Proceedings of the 15th International Symposium on the Packaging and Transportation of Radioactive Materials*, October 21–26, 2007, Miami, Florida (2007).

Chase, M.W., "JANAF Thermochemical Tables," 3rd Edition, Vol. 14, Washington, DC: American Chemical Society and the American Institute of Physics for the National Bureau of Standards (1985).

Churchill, S.W., H.H.S. Chu, "Correlating Equations for Laminar and Turbulent Free Convection From a Vertical Plate," *International Journal of Heat and Mass Transfer*, Vol. 18, p. 1,323 (1975).

Fluent, Inc., "FLUENT® Theory Guide Version 6.3," Lebanon, New Hampshire: Fluent, Inc. (2007a).

Fluent, Inc., "FLUENT® User Manual Version 6.3," Lebanon, New Hampshire: Fluent, Inc. (2007b).

Greiner, M. et al., "Use of Fuel Assembly/Backfill Gas Effective Thermal Conductivities to Predict Basket and Fuel Cladding Temperatures Within a Rail Package During Normal Transport," *Nuclear Technology*, Vol. 160, No. 3, pp. 325–336 (2007).

Gudipati, M., M. Greiner, "CFD Simulations of Fuel Cladding and Baslet Surface Temperatures in an MPC Rail Cask During Normal Transport," *Proceedings of the 15th International Symposium on the Packaging and Transportation of Radioactive Materials*, October 21–26, 2007, Miami, Florida (2007).

Heng, X. et al., "A Numerical Investigation of Natural Convection Heat Transfer in Horizontal Spent-Fuel Storage Cask," *Nuclear Engineering and Design*, Vol. 213, pp. 59–65 (2002).

Lee, J. et al., "Thermal-Fluid Flow Analysis and Demonstration Test of a Spent Fuel Storage System," *Nuclear Engineering and Design*, Vol. 239, pp. 551–558 (2009).

Li, J. et al., "Peak Cladding Temperature in a Spent Fuel Storage or Transportation Cask," *Proceedings of the 15th International Symposium on the Packaging and Transportation of Radioactive Materials*, October 21–26, 2007, Miami, Florida (2007).

McAdams, W.H., *Heat Transmission*, 3rd Edition, New York City, New York: McGraw Hill Book Company, Inc. (1954).

McKinnon, M.A. et al., "Performance Testing and Analyses of the VSC–17 Ventilated Concrete Cask," TR-100305, Electric Power Research Institute, Palo Alto, California (1992).

Nishimura, M. et al.,"Natural Convection Heat Transfer in the Horizontal Dry Storage System for the LWR Spent Fuel Assemblies," *Journal of Nuclear Science and Technology*, Vol. 33, pp. 821–828 (1996).

Shibazaki, H. et al., "A Study of Heat Transfer Characteristics for a Horizontal Dry Storage System for LWR Spent Fuel Assemblies," *Heat Transfer-Japan Research*, Vol. 27. pp. 284–298 (1998).

Takeda, H. et al., "Heat Removal Verification Tests Using Concrete Casks Under Normal Condition," *Nuclear Engineering and Design*, Vol. 238, pp. 1196–1205 (2008).

Walavalkar, A.Y., D.G. Schowalter, "3-D CFD Simulation of a Spent Nuclear Fuel Storage System," *American Nuclear Society*, Vol. 19, pp. 200–201 (2004).

Wataru, M. et al., "Thermal Hydraulic Analysis Compared with Tests of Full Scale Concrete Casks," *Nuclear Engineering and Design*, Vol. 238, pp. 1213–1219 (2008).

Wooton, R.O., H.M. Epstein, "*Heat Transfer from a Parallel Rod Fuel Element in a Shipping Container,*" Battelle Memorial Institute (1963).

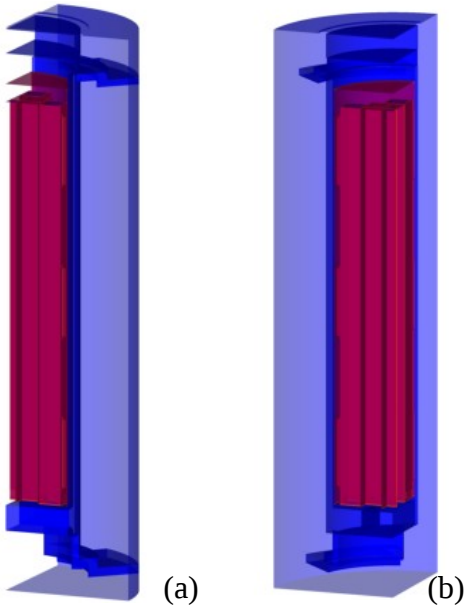

Fig. 1: Schematic of the computational domain

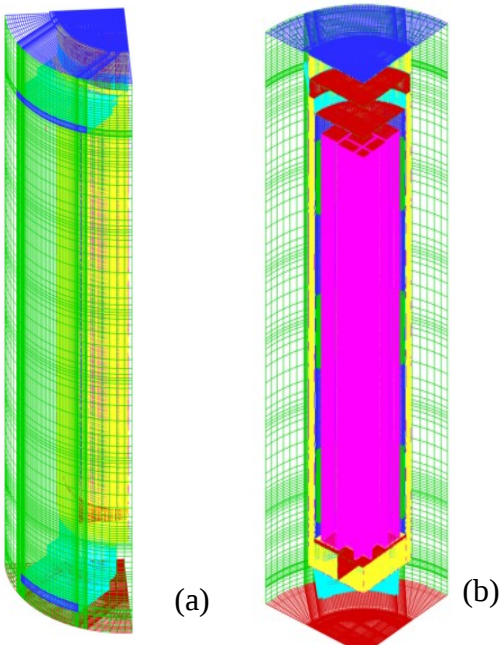

Fig. 2: VSC–17 cask with computational grid

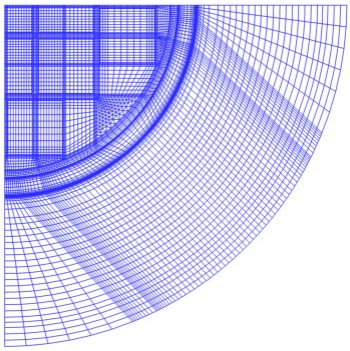

Fig. 3: Computational grid at the mid-vertical plane of the domain

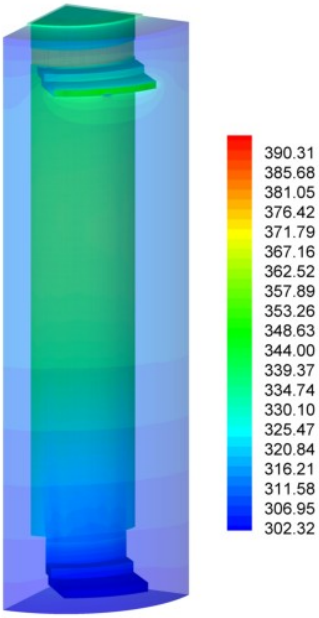

Fig. 5: Temperature contours (K) in the air passage and concrete shell

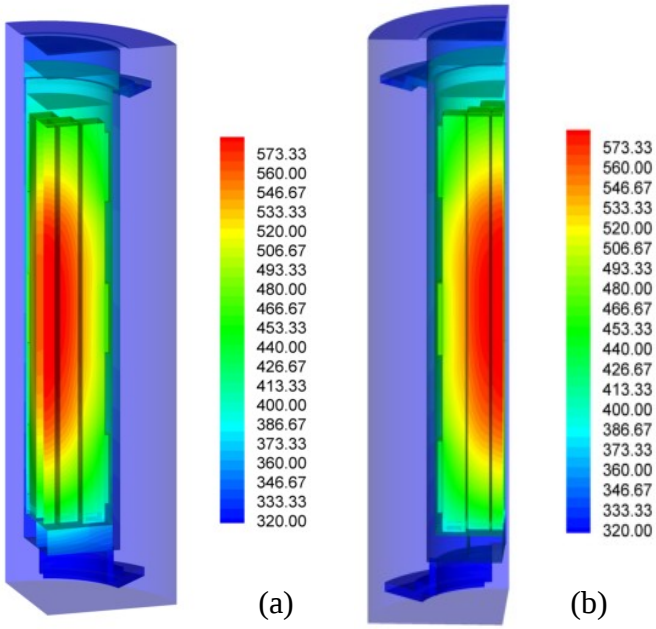

Fig. 4: Temperature contours (K) in the spent nuclear fuel canisters

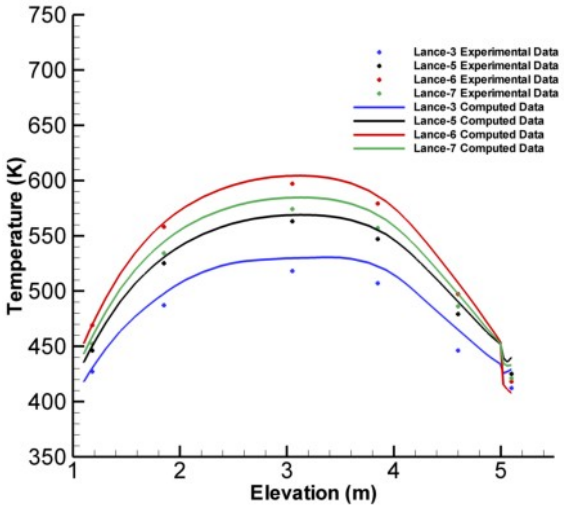

Fig. 6: Fuel axial temperature distribution for Case–1

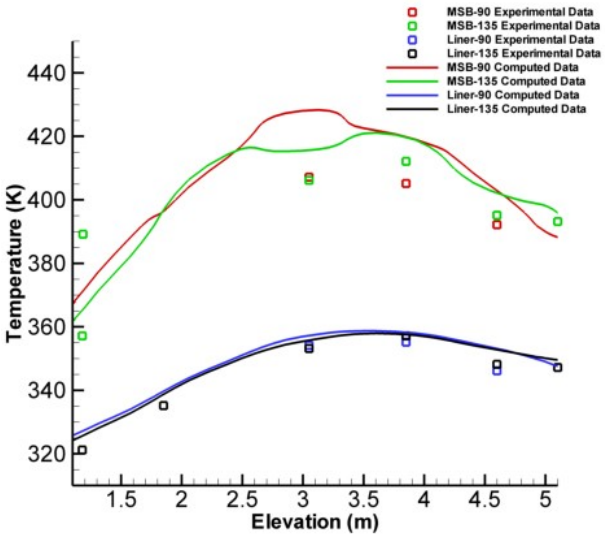

Fig. 7: Liner and multipurpose canister walls axial temperature distribution for Case–1

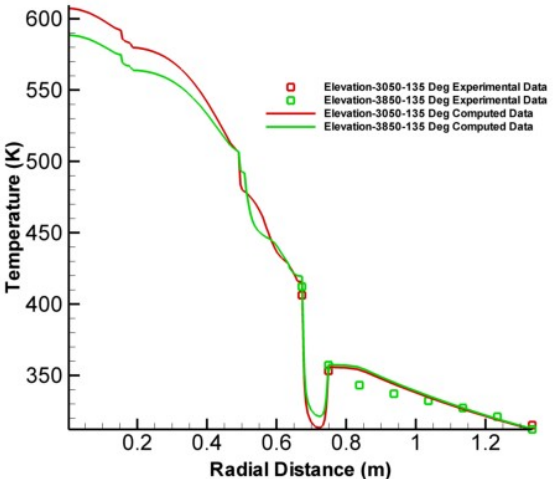

Fig. 8: Radial temperature distribution at two axial locations for Case–1

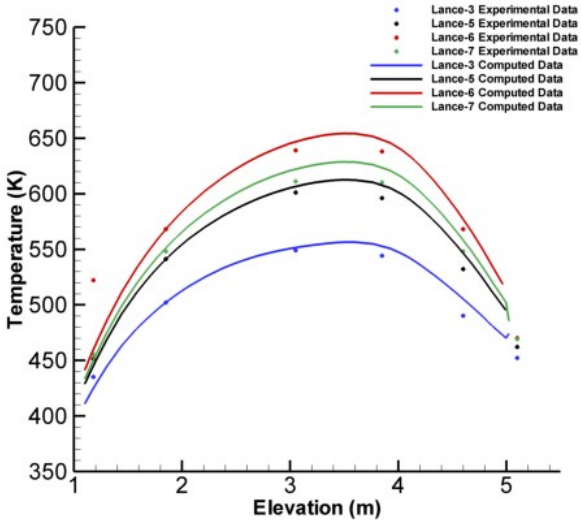

Fig. 9: Fuel axial temperature distribution for Case–2

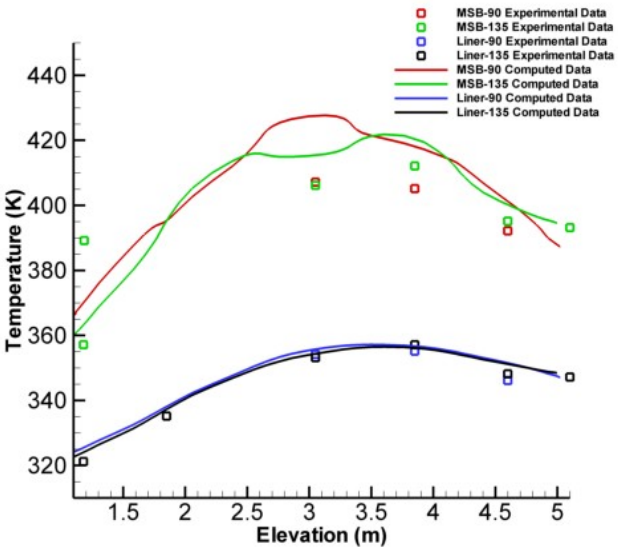

Fig. 10: Liner and multipurpose canister walls axial temperature distribution for Case–2

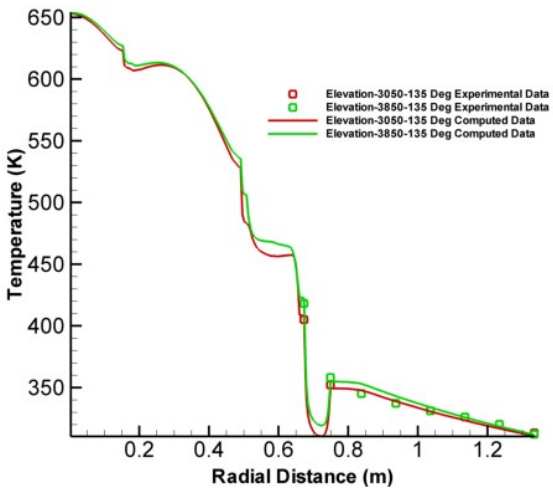

Fig. 11: Radial temperature distribution at two axial locations for Case–2

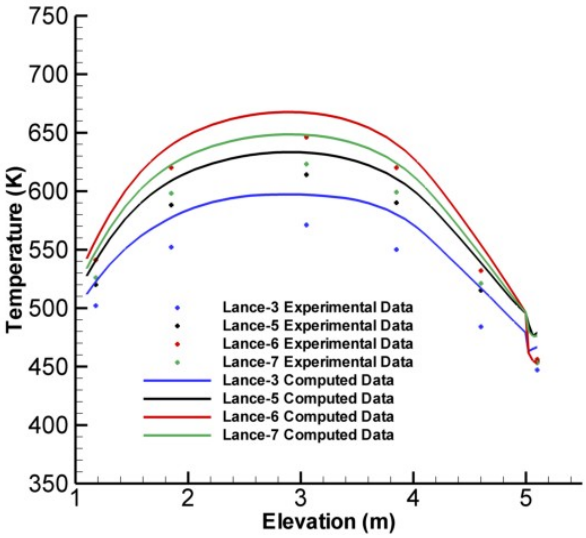

Fig. 12: Fuel axial temperature distribution for Case–3

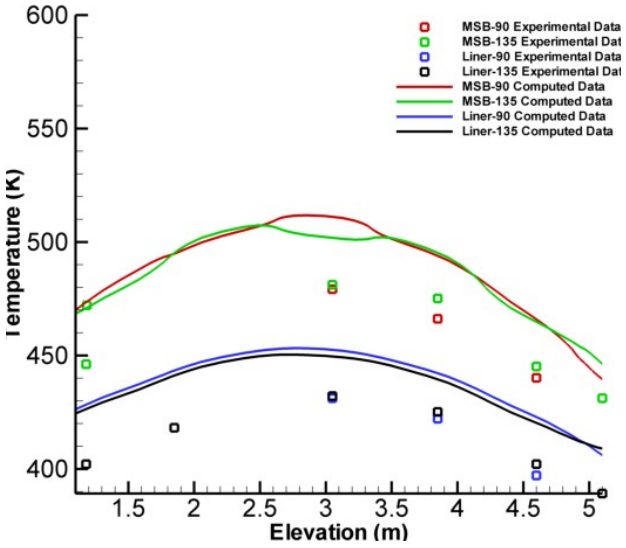

Fig. 13: Liner and multipurpose canister walls axial temperature distribution for Case–3

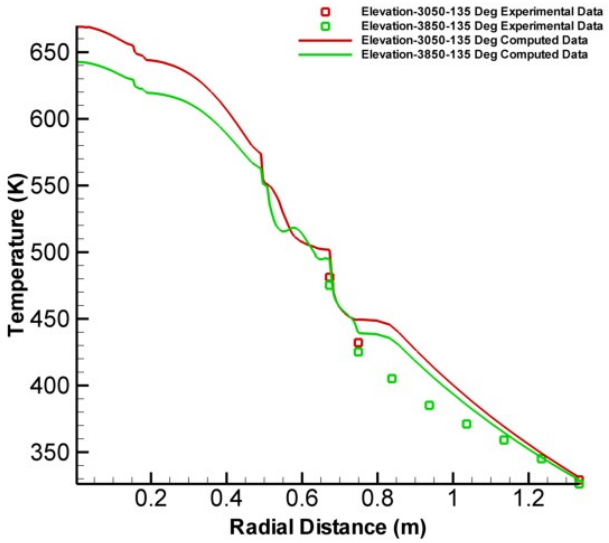

Fig. 14: Radial temperature distribution at two axial locations for Case–3

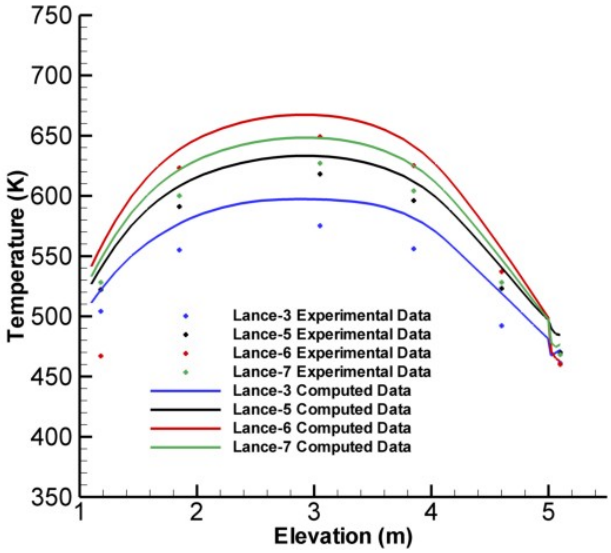

Fig. 15: Fuel axial temperature distribution for Case–4

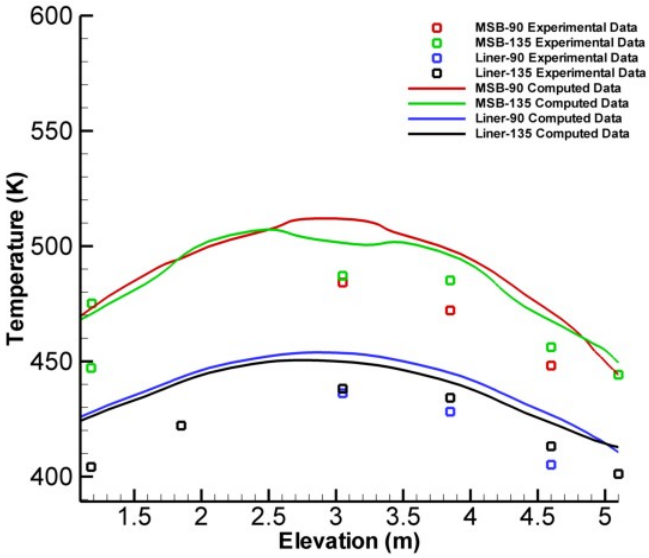

Fig. 16: Liner and multipurpose canister walls axial temperature distribution for Case–4

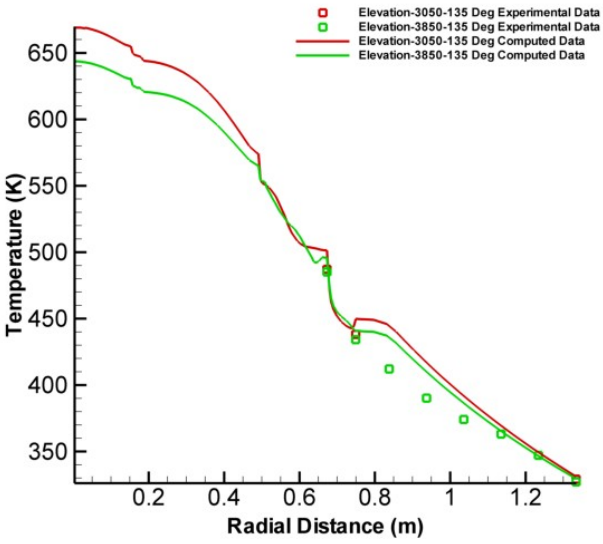

Fig. 17: Radial temperature distribution at two axial locations for Case–4

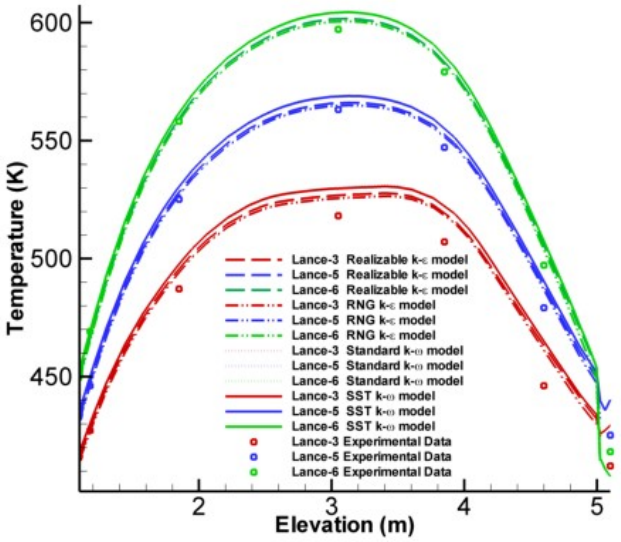

Fig. 18: Fuel axial temperature distribution predicted by different turbulence models

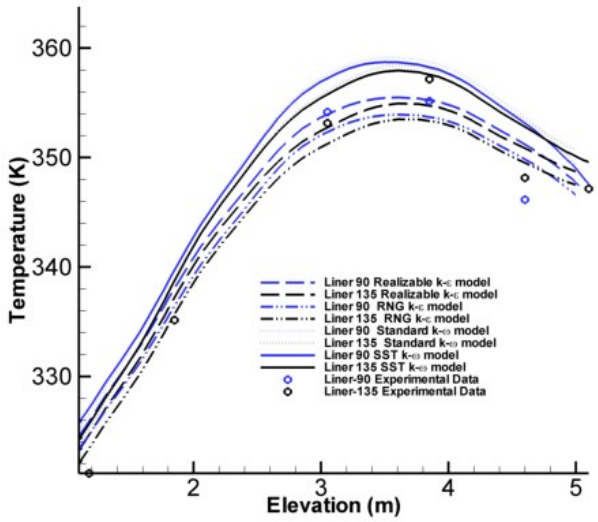

Fig. 19: Multiassembly sealed basket temperature distribution for different turbulence models

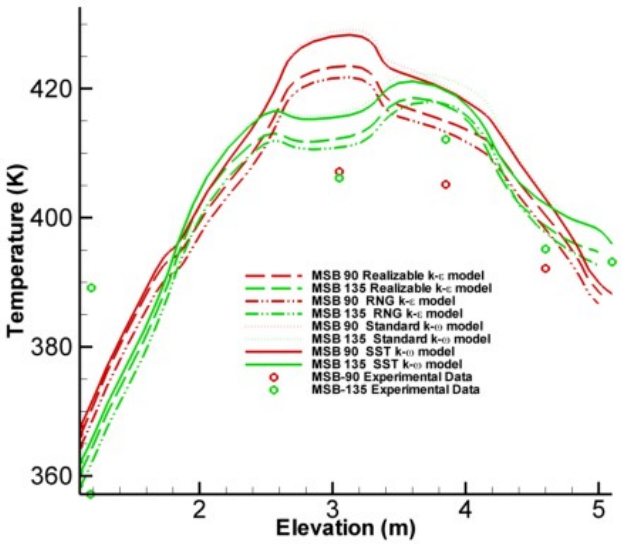

Fig. 20: Liner temperature distribution for different turbulence models

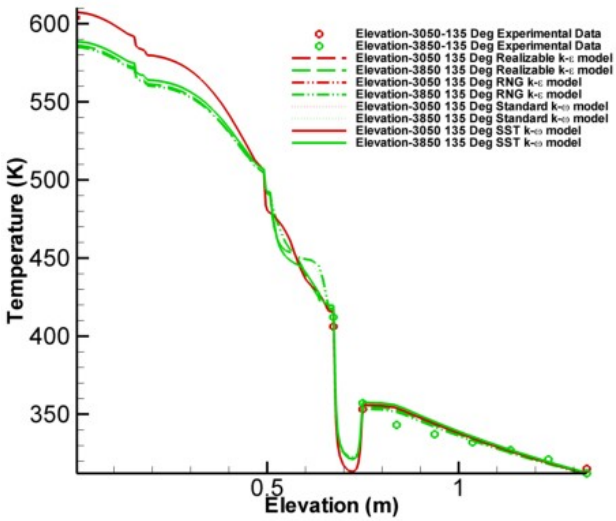

Fig. 21: Radial temperature distribution for different turbulence models